INTERNATIONAL JOURNAL FOR NUMERICAL METHODS IN FLUIDS, VOL. 9, 1369–1379 (1989)

# A COMPARISON OF PRIMITIVE VARIABLES AND STREAMFUNCTION–VORTICITY FOR FEM DEPTH-AVERAGED MODELLING OF STEADY FLOW

BRUCE A. DeVANTIER

*Department of Civil Engineering and Mechanics, Southern Illinois University, Carbondale, IL 62901, U.S.A.*

## SUMMARY

The governing equations for depth-averaged turbulent flow are presented in both the primitive variable and streamfunction–vorticity forms. Finite element formulations are presented, with special emphasis on the handling of bottom stress terms and spatially varying eddy viscosity. The primitive variable formulation is found to be preferable because of its flexibility in handling spatial variation in viscosity, variability in water surface elevations, and inflow and outflow boundaries. The substantial reduction in computational effort afforded by the streamfunction–vorticity formulation is found not to be sufficient to recommend its use for general depth-averaged flows. For those flows in which the surface can be approximated as a fixed level surface, the streamfunction–vorticity form can produce results equivalent to the primitive variable form as long as turbulent viscosity can be estimated as a constant.

KEY WORDS Depth-averaged flow Finite elements Streamfunction–vorticity

## INTRODUCTION

With the advent of more and more powerful desk-top computers, it is now possible to model complex recirculating natural flows in the setting of a small consulting firm's office. Two-dimensional (2D) shallow water flows are of greater interest in this regard because of their significance in environmental engineering, oceanography and coastal engineering, to name a few examples. These 2D flows are most often turbulent, and so the modeller must utilize models and numerical solution approaches somewhat different from laminar flow models. The limits of numerical flow modelling techniques are sorely tested by the demands of many of the turbulence models currently in vogue.

Two important yet competing criteria in the development of this type of numerical flow model are: (1) maintaining reasonable computer central processing unit (CPU) time utilization and (2) obtaining numerical results which can reasonably approximate the solution of the continuum governing equations which are being modelled. The choice between the primitive variable and the streamfunction–vorticity formulation of 2D momentum conservation for an incompressible fluid involves these criteria and is the basis of subsequent discussion.

## BACKGROUND

Governing equations for prediction of flow velocities in steady depth-averaged turbulent flow have been given by McGuirk and Rodi[1] and are presented in the following two momentum

0271–2091/89/111369–11$05.50

*Received 6 November 1987*
*Revised 23 August 1988*

conservation equations along with a conservation of mass equation as

$$U\frac{\partial U}{\partial x}+V\frac{\partial U}{\partial y}=-g\frac{\partial}{\partial y}(h+z_b)+\frac{1}{\rho h}\frac{\partial}{\partial x}(h\bar{\tau}_{xx})+\frac{1}{\rho h}\frac{\partial}{\partial y}(h\bar{\tau}_{xy})+\frac{1}{\rho h}(\tau_{sx}-\tau_{bx}), \tag{1}$$

$$U\frac{\partial V}{\partial x}+V\frac{\partial V}{\partial y}=-g\frac{\partial}{\partial y}(h+z_b)+\frac{1}{\rho h}\frac{\partial}{\partial x}(\bar{\tau}_{xy})+\frac{1}{\rho h}\frac{\partial}{\partial y}(h\bar{\tau}_{yy})+\frac{1}{\rho h}(\tau_{sy}-\tau_{by}), \tag{2}$$

$$\frac{\partial}{\partial x}(hU)+\frac{\partial}{\partial y}(hV)=0, \tag{3}$$

where $x$, $y$, $U$ and $V$ are the co-ordinate directions and their corresponding depth-averaged velocity components. The equations result from averaging the full three-dimensional equations through integration over the vertical depth. A distinction is therefore made between the depth-averaged stress terms ($\bar{\tau}_{xx}$, $\bar{\tau}_{yy}$ and $\bar{\tau}_{xy}$) and boundary stresses ($\tau_{sx}$, $\tau_{bx}$, $\tau_{sy}$ and $\tau_{by}$), where the former result from their planar counterparts while the latter are surface and bottom stress components evaluated at the limits of the depth integration. The depth of water at a given point is $h$, and $z_b$ is the distance of the bottom boundary from an arbitrary datum. Gravitational acceleration $g$ acts normal to the $x$–$y$ plane, and consideration of variations in density $\rho$ is not included.

The equation set (1)–(3) is not closed without a model of the stress terms. In this paper the eddy viscosity will be utilized in closure of the equation set because of its wide use. The depth-averaged stresses thus become

$$\frac{\bar{\tau}_{xx}}{\rho}=2\nu_t\frac{\partial U}{\partial x}, \qquad \frac{\bar{\tau}_{yy}}{\rho}=2\nu_t\frac{\partial V}{\partial y}, \qquad \frac{\bar{\tau}_{xy}}{\rho}=\nu_t\left(\frac{\partial U}{\partial y}+\frac{\partial V}{\partial x}\right), \tag{4}$$

where $\nu_t$ is a depth-averaged eddy viscosity. In tensor form these become

$$\frac{\tau}{\rho}=\nu_t(\nabla\mathbf{v}+\nabla\mathbf{v}^T), \tag{5}$$

where $\mathbf{v}$ is the velocity vector, with the superscript T denoting the transpose of the tensor.

The governing equations cannot be transformed to the familiar form of the vorticity transport equation unless the physical setting considered is limited to a nearly flat bottom boundary ($z_b=0$ everywhere) and the flow depth is nearly constant everywhere. This assumption is sometimes called the rigid lid assumption. While this is a significant restriction, there are quite a number of practical situations in which this may be assumed. Still, this limitation is a negative aspect of streamfunction–vorticity formulations of the class of problems considered here. The vorticity transport equation is somewhat different than that for laminar flow, and in tensor form it is

$$\mathbf{v}\cdot\nabla\omega=\nabla\cdot(\nu_t\nabla\omega)+\nabla\cdot\left(\frac{1}{\rho h}(\boldsymbol{\tau}_s-\boldsymbol{\tau}_b)\right)+\nabla\cdot[\nabla\nu_t\times(\nabla\mathbf{v}+\nabla\mathbf{v}^T)]. \tag{6}$$

Note that $\boldsymbol{\tau}_s$ and $\boldsymbol{\tau}_b$ are now vector quantities as well as the vorticity $\omega$, but since only 2D flow is assumed, its scalar magnitude is

$$\omega=|\nabla\times\mathbf{v}| \tag{7}$$

At this point the surface and bottom stress term will be simplified for presentation purposes, because $\boldsymbol{\tau}_s$ and $\boldsymbol{\tau}_b$ are treated similarly. Further equations will consider only bottom stress and utilize the following friction coefficient ($C_f$) formulation:

$$\boldsymbol{\tau}_b = C_f\mathbf{v}(\mathbf{v}\cdot\mathbf{v})^{1/2}. \tag{8}$$

The last two terms of equation (6) represent the difference from the form of the vorticity transport equation for laminar flow of a Newtonian fluid. The origin of the first extra term is apparent when it is remembered that the vorticity transport equation is generated by taking a cross product of the del operator and the vector momentum equation. The other extra term has a similar origin but is also the result of allowing $\nu_t$ to vary spatially, as is generally the case in practice. It is not uncommon (see Oliver,[2] for example) to ignore this term in finite difference solutions of the vorticity equation. The extent of errors associated with ignoring the term will depend upon the variability of $\nu_t$ and the mesh refinement.

The solution for depth-averaged flow velocities is often not the end goal of the modeller. The velocities may then be used to determine movement of contaminants, tendency towards bottom scour and other secondary variable determinations. A general transport equation typical of those described is

$$\mathbf{v}\cdot\nabla\phi=\nabla\cdot(\alpha_t\nabla\phi)+s/\rho h. \tag{9}$$

Here $\phi$ is a scalar contaminant, $s$ is a volume-distributed source of $\phi$, and $\alpha_t$ is the turbulent diffusivity of the flow. The turbulent diffusivity is of the same order as the turbulent viscosity and is often taken to have the same value locally.

## FINITE ELEMENT FORMULATIONS

With the simplifications described previously, the element level residual equations for the primitive variable form of the governing equations using a Galerkin formulation are

$$R_{1i}=\int_{\Omega_e} N_i[\mathbf{v}\cdot\nabla\mathbf{v}+g\nabla h-C_f\mathbf{v}(\mathbf{v}\cdot\mathbf{v})^{1/2}]\,\mathrm{d}\Omega + \int_{\Omega}\nabla N_i\cdot\nabla\cdot[\nu_t(\nabla\mathbf{v}+\nabla\mathbf{v}^{\mathrm{T}})]\,\mathrm{d}\Omega-\int_{\Gamma_e} N_i\nu_t(\nabla\mathbf{v}+\nabla\mathbf{v}^{\mathrm{T}})\cdot\mathbf{n}\,\mathrm{d}\Gamma, \tag{10}$$

$$R_{2i}=\int_{\Omega_e} M_i\nabla\cdot\mathbf{v}\,\mathrm{d}\Omega, \tag{11}$$

where $\Omega_e$ and $\Gamma_e$ are the element interior domain and boundary respectively. The form of these nodal residuals ($i$ corresponds to node $i$) follows the form of Hood and Taylor[3] as modified by Schamber and Larock[4] for spatially varying viscosity flows. The nodal variable $\mathbf{v}$ is interpolated biquadratically with Lagrangian shape factors as

$$\mathbf{v}=\sum_j (N_j\mathbf{v}_j) \tag{12}$$

and $h$ is interpolated bilinearly with a different shape factor $M_i$ as

$$h=\sum_j (M_j h_j). \tag{13}$$

It is important here to note that $h$ appears only as $\nabla h$ in equation (10) and does not appear in equation (11). This is due to the rigid lid assumption, and so only the slight variations in depth about the uniform depth need to be calculated in $h$.

Before the streamfunction–vorticity residuals can be defined, the streamfunction $\Psi$ must be defined indirectly by its derivatives as

$$U=\partial\Psi/\partial y, \qquad V=-\partial\Psi/\partial x, \tag{14}$$

so that the constraint equation resulting from the definition of $\omega$ is

$$\omega = -\nabla^2\Psi. \tag{15}$$

Following Campion-Renson and Crochet[5] as later expanded by Peeters *et al.*[6], the Galerkin residuals can be written as

$$R^{\cdot}_{1i} = \int_{\Omega_e} [N_i \nabla\omega \cdot \nabla\Psi + \nabla N_i \cdot (v_t \nabla\omega)]\, d\Omega - \int_{\Gamma_e} N_i \nabla\omega \cdot \mathbf{n}\, d\Gamma + \int_{\Omega_e} N_i \nabla \cdot [C_f \mathbf{v}(\mathbf{v}\cdot\mathbf{v})^{1/2}]\, d\Omega, \tag{16}$$

$$R^{\cdot}_{2i} = \int_{\Omega_e} (\nabla N_i \cdot \nabla\Psi - N_i\omega)\, d\Omega - \int_{\Gamma_e} N_i \nabla\Psi \cdot \mathbf{n}\, d\Gamma. \tag{17}$$

The advantage of this form of solution for the independent variables $\Psi$ and $\omega$ is that specification of $\Psi$ results in no need for specification of the boundary integral of equation (16), and specification of the velocity tangential to a boundary is considered through the boundary integral of equation (17). Note that the same quadratic weighting and shape function $N_i$ is used in equations (16) and (17). This differs from the preferred formulation of Peeters *et al.*[6] in that $\Psi$ and $\omega$ are both interpolated quadratically rather than $\omega$ linearly and $\Psi$ quadratically, but further discussion of this difference will be deferred until the discussion of model results.

The last term of equation (16) is not compatible with the $C^0$-continuous interpolation functions, because secondary derivatives of the primary variable $\Psi$ appear in it. Upon applying the usual Green's transformation and substituting for velocity in terms of $\Psi$, this term may be written

$$\int_{\Omega_e} N_i |\nabla \times [C_f \mathbf{v}(\mathbf{v}\cdot\mathbf{v})^{1/2}]|\, d\Omega = -\int_{\Omega_e} \nabla\Psi \times \nabla N_i C_f (\nabla\Psi \cdot \nabla\Psi)^{1/2}\, d\Omega + \int_{\Gamma_e} C_f N_i \nabla\Psi \times \mathbf{n}(\nabla\Psi \cdot \nabla\Psi)\, d\Gamma.$$

The boundary integral introduced in equation (18) is not evaluated on specified $\Psi$ boundaries, and on inflow or outflow boundaries the integral will be zero if the velocity tangential to the outflow boundary is specified as zero. An alternative to the substitution of equation (18) into equation (16) can be considered if spatial variations in $\mathbf{v}\cdot\mathbf{v}$ can be taken as negligible with respect to spatial variations in $U$ or $V$ (this will not be true for strongly swirling or accelerated flows). The following approximation will then be applicable:

$$\int_{\Omega_e} N_i |\nabla \times [C_f \mathbf{v}(\mathbf{v}\cdot\mathbf{v})^{1/2}]|\, d\Omega \approx \int_{\Omega_e} N_i C_f (\nabla\Psi \cdot \nabla\Psi)\, \omega\, d\Omega. \tag{19}$$

An advantage of this form is the lack of boundary integrals to be considered; furthermore, it is less non-linear than the more complete form.

Both the primitive variable equation set and the streamfunction–vorticity set are non-linear. Newton–Raphson iteration is used to obtain converged solutions utilizing the full Newton–Raphson step in the primary variables.

## RESULTS

Two flow geometries which have been examined extensively in computing laminar flow, the driven cavity and flow over a step, have been chosen for the comparison of the two forms. The driven cavity is a square region in which three walls are fixed and one side wall moves with a constant velocity. The step flow is described by a specified velocity profile through a channel of constant width, after which the channel abruptly expands to double its width.

In the context of depth-averaged flow the driven cavity can be used as a model of a stilling region next to a river, and step flow is an abrupt expansion of a rectangular channel. The velocity

profiles of the depth-averaged flow computations reduce to the standard cavity and step cases as $C_f$ goes to zero or $h$ grows large.

As noted earlier, the form of solution of the $\Psi$–$\omega$ set is somewhat different than the unequal-order interpolation scheme of Peeters *et al.*[6] As a basis for comparison, creeping cavity flow was calculated using the unequal as well as equal-order interpolation forms. The creeping flow is forced by assuming that $\nu_t$ is much larger than the moving wall velocity, so that the Reynolds number based on a constant $\nu_t$, the moving wall velocity and the cavity length goes to zero. $C_f$ was set to zero and thus the problem becomes linear, and the Newton–Raphson method converges in one iteration. Utilizing a fine mesh of 196 ($14 \times 14$) elements, the results of the two methods were virtually indistinguishable, but the computation time was significantly less for the unequal interpolation. A plot of vorticity contours is shown in Figure 1. While this plot agrees with that of Campion-Renson and Crochet,[5] it is worth examining in closer detail. An expanded view of the upper right-hand corner of Figure 1 is shown in Figure 2. The extreme fluctuations of $\omega$ cannot be cured by mesh refinement, but are due to the inability of $\nabla^2\Psi$ to define $\omega$ near the corner where the derivative of $\Psi$ is discontinuous, as pointed out by Fix.[7] Thus the wiggles exist for both equal and unequal interpolation forms, and conservation of mass is less accurate near the corner as a result. It should be noted though that global conservation is still ensured through the specification of a constant value of $\Psi$ along the border. A possible resolution of the problem would be use of $C^1$-continuous interpolation at least at element boundaries, as proposed by Utka and Carey.[8] This penalty form could not be used here, however, because continuity is not enforced on global boundaries. The usual form of use of the higher-order continuity defeats one of the basic advantages of $\Psi$–$\omega$ forms in that more nodal unknowns are introduced.

Figure 3 compares the horizontal velocity predictions of the $\Psi$–$\omega$ and the $U$–$V$–$h$ forms across the midplane of the cavity for a flow with spatial variation in $\nu_t$. The previous element mesh was used for both calculations. The viscosity is arbitrarily specified, with $\nu_t$ equivalent to a cavity Reynolds number of 1000 at the walls, increasing quadratically to create a local Reynolds number of 10 at the centre. Although arbitrary, the eddy viscosity distribution has near-wall variation

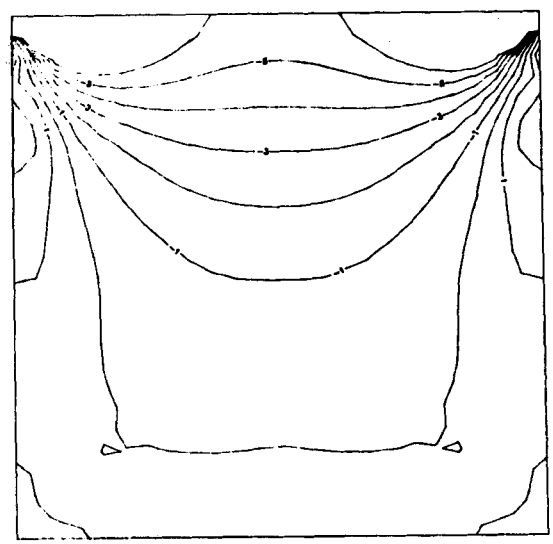


Figure. 1. Vorticity contours for zero-Reynolds-number cavity flow

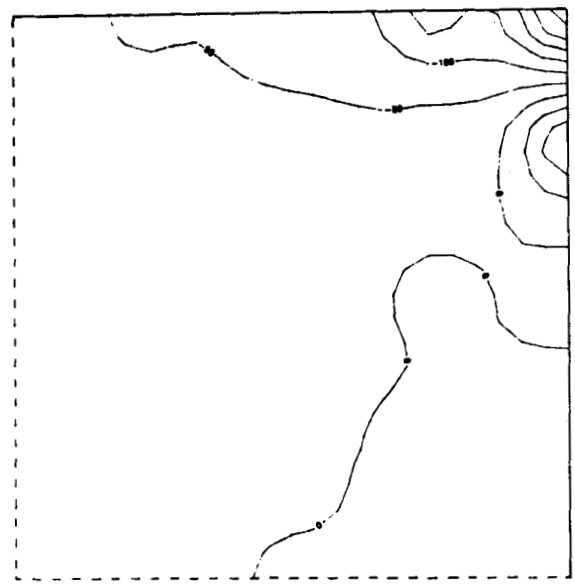

Figure 2. Expanded corner view of zero-Reynolds-number vorticity for a cavity.

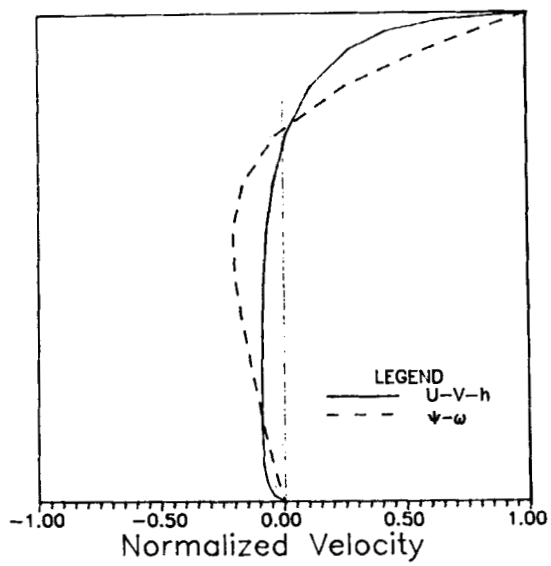


Figure 3. Comparison of mid-cavity velocity profiles for spatially varying viscosity

similar to that observed experimentally, in the sense that the lowest viscosities appear nearest the walls and the viscosity increases rapidly away from the walls. The $\Psi$–$\omega$ solution cannot adequately resolve the effect of variation in $\nu_t$ upon velocity, as evidenced by the more nearly parabolic lower portion of the profile. One of the causes of this effect is that the last term of equation (6) was neglected. This term could not be included unless higher-order continuity were introduced, because of the higher-order derivatives in the term. Another reason for the difference

in profiles is that the $\Psi$–$\omega$ equation set could not be made to converge stably unless a single averaged value of $\nu_t$ was taken for each element. The velocity profile for the $U$–$V$–$h$ solution is as expected in that the strong increase in $\nu_t$ away from the wall produces a flow parallel to the wall opposite from the moving wall, which is similar to turbulent channel flow with the strongest gradients nearest the wall. One might also expect this type of profile, because channel flow profiles of turbulent viscosity have been found experimentally to be parabolic normal to the wall. It should be made clear though that actual turbulent flow profiles for driven cavity flow are significantly different,[9] because the turbulent viscosity field is not symmetric about the cavity centre as specified in this test calculation.

The $\Psi$–$\omega$ prediction for the variable viscosity case was made to more nearly approach the $U$–$V$–$h$ prediction when the row of elements adjacent to the moving boundary was subdivided into two rows. The predictions came very close when a further subdivision was made, although the zero-velocity point was approximately 0·05 of a cavity width lower. These results merely reflect the fact that mesh refinement in high-gradient areas will generally improve a solution. The results may also be interpreted to indicate that the primary error introduced in $\Psi$–$\omega$ modelling of variable viscosity flows is due to the assumption of constant $\nu_t$, rather than the omission of the last term of equation (6). This should be true of nearly all flows, because $\nabla\nu_t$ will nearly always be significant in the same vector direction as the major components of the velocity shear tensor, with which it has a cross product in the omitted term. This is because the highest viscosity variations normally appear near boundaries where flow is nearly parallel to the boundary, and because the greatest gradients are normal to the boundary.

The capability of the two forms to predict bottom friction effects was tested by using a friction coefficient of 0·01 with a flow depth 0·1 times the length of the cavity side and a constant eddy viscosity producing a cavity Reynolds number of 400. Both forms were able to predict the flattening of the velocity gradients due to the bottom drag. Figure 4 is a comparison of the centreline velocity profile with and without the drag. The curves are valid for both $\Psi$–$\omega$ and $U$–$V$–$h$ solutions within 0·1%, and it should be noted that the modified form of the bottom term

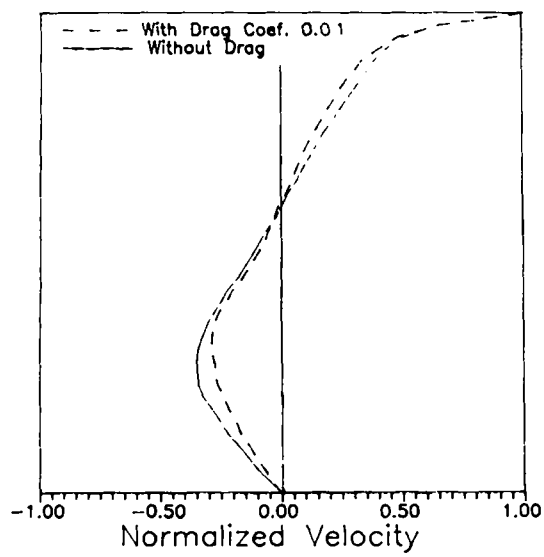


Figure. 4. Comparison of mid-cavity profiles with and without bottom drag

from equation (19) in the $\Psi$–$\omega$ form was within 0·5% of the plotted profile. Given the inaccuracy of determining $C_f$ in practice, the approximation appears acceptable.

The velocity fields predicted above were used in a contaminant transport prediction using the same computational grid as the velocity predictions. Equation (9) was solved using nine-node quadratic interpolation for $\phi$ with the source $s$ taken as a linear function of $\phi$. The form of the source term is taken as a first-order decay given by

$$s = -k\phi. \tag{20}$$

A uniform distributed flux of $\phi$ was applied along the moving wall of the cavity. The predictions of $\phi$ were very close using both $U$–$V$–$h$ and $\Psi$–$\omega$ to determine the convective velocities. Both forms exhibited global conservation of $\phi$ to within 0·1%, which is not surprising because of the fine mesh used and a conservative form of the convection term in the finite element equations (in the form of flux terms as suggested by Gresho *et al.*[10]).

It was found however that the form of boundary condition applied using the $U$–$V$–$h$ form affected global conservation of the contaminant. Figures 5 and 6 are predictions of $\phi$ contours for which two different forms of specification of moving wall velocity were applied in the $U$–$V$–$h$ solutions. For the first, the corner node velocities were set to zero, while for the second, $U$ was set to the moving wall velocity and $V$ to zero. As noted by Hughes *et al.*,[11] velocity predictions are slightly different depending upon the form used, and Figure 7 illustrates the problem with the second form. Flow is actually allowed to 'leak' out of the fixed wall when quadratic interpolation is forced through two-velocity nodes and one non-zero-velocity node. Even though a very small corner element was used (0·025 × 0·025 based on cavity length), the first-order decay term accounted for only 95% of the flux of $\phi$ specified. It is also interesting to note that the 'leaky' boundary condition produces instability in the $\phi$ solution, as indicated by the wiggles in the fingers protruding from the upper right-hand corner of Figure 6. The velocities normal to the moving wall switch sign in a periodic fashion as the corner is approached.

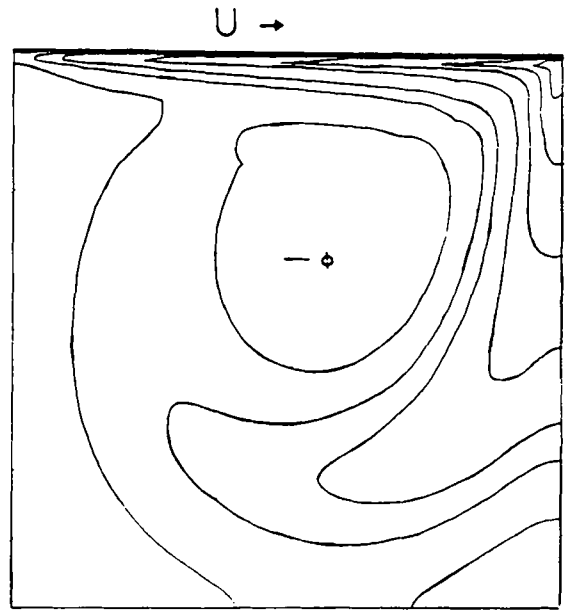


Figure 5. Contaminant concentration contours for driven cavity flow with no flow out of cavity

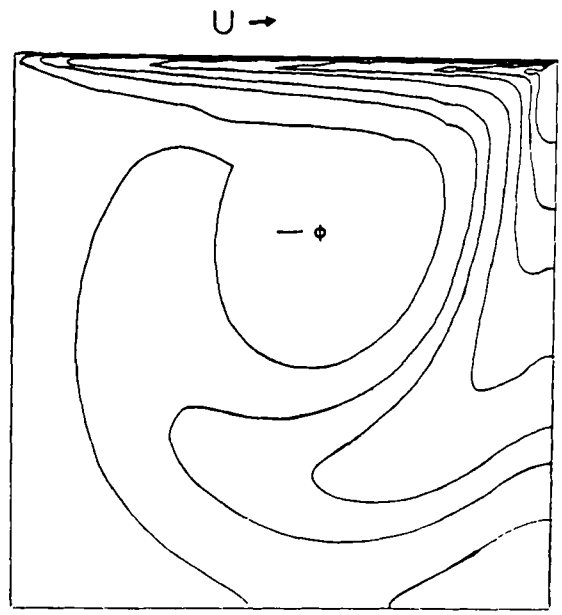


Figure 6. Contaminant concentration contours for cavity flow with interpolated flow out of cavity

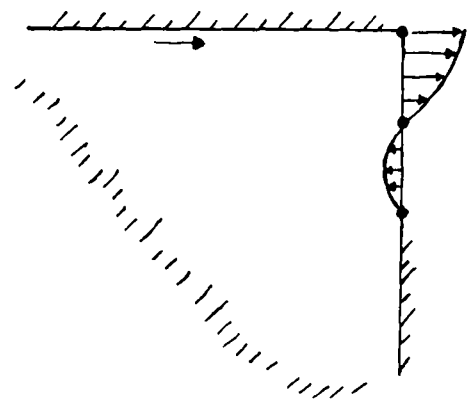

Figure 7. Interpolation resulting in flow out of the cavity

The $\Psi$–$\omega$ form did not fare so well in comparison when the flow was not completely enclosed. Figure 8 is a plot of $\Psi$ contours for flow through a channel expansion of Reynolds number 133 based on the upstream channel width and a constant eddy viscosity. Note that the separation streamline reattaches near 6·0 step heights downstream and that the $U$–$V$–$h$ reattachment point shown by the X is farther downstream. The reason for the difference is the presence of streamline curvature around the separation corner. The inability of the $\Psi$–$\omega$ form to satisfy equation (15) near this corner, at which the normal derivative of $\Psi$ becomes undefined, allows this to occur. Thus the problem was consistent at all flows and was accentuated for higher Reynolds numbers as demonstrated by Figure 9. The primitive variable predictions agree with many published predictions (see Polansky *et al.*[12]) for a completely developed inlet flow.

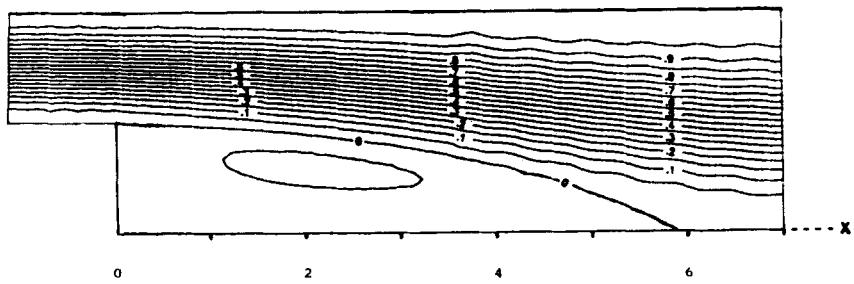


Figure 8. Streamlines for flow through an asymmetric expansion with streamfunction–vorticity form

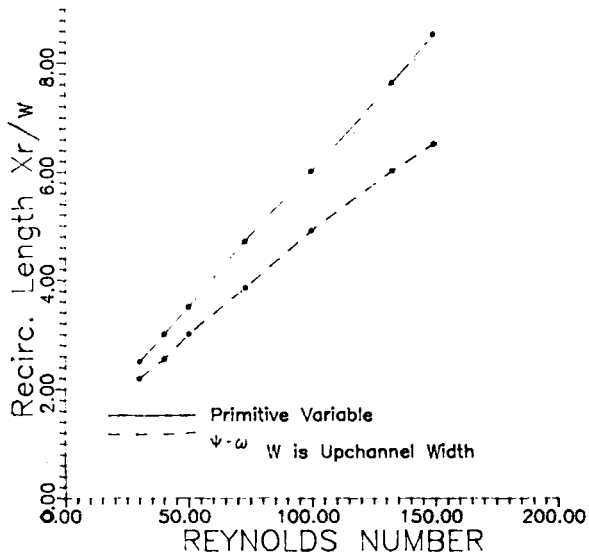


Figure 9. Reattachment length predicted by primitive variable and streamfunction–vorticity forms

The $\Psi$–$\omega$ predictions were made to agree with the $U$–$V$–$h$ predictions when $\Psi$ was specified as the same value as the upstream wall value one node out into the flow past the expansion. This is equivalent to the specification of separation streamlines sometimes used in finite difference calculations. It is not a pleasing alternative in general, however, because the direction of the separation streamline is not necessarily known for more oblique corner angles; furthermore, it requires that separation at such corners be assumed *a priori*.

## CONCLUSIONS

It is clear that the depth-averaged form of the momentum equations for turbulent flows require special handling for FEM solution, especially with regard to the bottom shear terms. Two mathematical descriptions have been presented, and it is felt that they perform satisfactorily in properly modelling bottom effects using either the momentum or vorticity description. It may be concluded that, for this class of flow prediction problem, the primitive variable form of description is to be preferred over streamfunction–vorticity when FEM solution is employed. The reasons for

the preference are difficulties in the $\Psi$–$\omega$ approach in properly dealing with spatial variation in turbulent viscosity, difficulties in dealing with prescribed inflow boundary conditions and the inability to describe spatial variations in water surface elevations. The significant savings in computational effort (as compared to that of primitive variable solution) cannot compensate for the deficiencies described.

ACKNOWLEDGEMENT

This research has been supported by the Department of the Interior's Mineral Institutes program administered by the Bureau of Mines under allotment grant number G116 4117.

REFERENCES

1. J. J. Mcguirk, and W. Rodi, 'A depth-averaged mathematical model for the near field of side discharges into open channel flow', *J. Fluid Mech.*, **86,** 761–768 (1978).
2. A. J. Oliver, 'The prediction of turbulent flow and heat transfer over backward facing steps', in *Computer Methods in Fluids*, Pentech Press, London, 1980, pp. 309–338.
3. P. Hood and C. Taylor, 'Navier Stokes equations using mixed interpolation', in *Finite Element Methods in Flow Problems*, UAH Press, Alabama, 1974, pp. 121–132.
4. D. R. Schamber and B. E. Larock, 'Numerical analysis of flow in sedimentation basins', *J. Hydraul. Div., ASCE*, **107,** 575–591 (1981).
5. A. Campion-Renson and M. Crochet, 'On the stream function–vorticity finite element solutions of the Navier–Stokes equations', *Int. j. numer. methods eng.*, **12,** 1809–1818 (1978).
6. M. F. Peeters, W. G. Habashi and E. G. Dueck, 'Finite element stream function–vorticity solutions of the incompressible Navier–Stokes equations', *Int. j. numer. methods fluids*, **7,** 17–27 (1987).
7. G. Fix, 'Finite element approximations to flow problems', *Proc. Third Int. Conf. on Finite Elements in Water Resources*, Ag. Research, USDA, New Orleans, 1980, pp. 4.3–4.13.
8. M. Utka and G. F. Carey, 'Stream function solution to Navier–Stokes problems with inter-element penalties', *Int. j. numer. methods fluids*, **7,** 191–193 (1987).
9. B. E. Launder, *Turbulence Transport Models for Numerical Computation of Fluid Flow*, University of California, Davis, Department of Mechanical Engineering, 1976.
10. P. M. Gresho, R. L. Lee, R. L. Sani, M. K. Maslanik and B. E. Eaton, 'The consistent Galerkin FEM for computing derived boundary quantities in thermal and/or fluids problems', *Int. j. numer. methods fluids*, **7,** 371–394 (1987).
11. T. J. R. Hughes, W. K. Liu and A. Brooks, 'Finite element analysis of incompressible viscous flows by the penalty formulation', *J. Comput. Phys.*, **30,** 1–60 (1979).
12. G. F. Polansky, J. P. Lamb and D. E. Klein, 'A finite element analysis of incompressible laminar and turbulent flow with heat transfer', in G. F. Carey and J. T. Oden (eds), *Proc. Fifth Int. Symp. on Finite Elements and Flow Problems*, 1984, pp. 243–247.